ACS APPLIED OPTICAL MATERIALS

pubs.acs.org/acsaom

Article

All-Optical Reconfigurable WGM Microcavities in Azodendrimer-Doped Liquid Crystals

Asish P. Venkitesh, Ramesh Manda, Osamu Haba, and Surajit Dhara*

Cite This: ACS Appl. Opt. Mater. 2025, 3, 2841−2847

Read Online

ACCESS | Metrics & More | Article Recommendations

ABSTRACT: We report on all-optical reconfigurable whispering gallery mode microcavities based on azodendrimer-doped liquid crystal (LC) microdroplets. The incorporated azodendrimer molecules, bearing multiple azobenzene chromophores, undergo reversible trans−cis photoisomerization under UV/visible illumination (~4.5 mW/cm^2). The molecular switching induces a significant realignment of the liquid crystal director field, which takes approximately 10 s to transition from a radial to a bipolar configuration and approximately 30 s for the reverse transition, resulting in substantial and reversible modulation of the refractive index ($\simeq$ 0.11). The resulting shifts in the WGM spectra are about a few nanometers and can be cycled repeatedly. This dynamic all-optical modulation enables real-time, reversible switching of the microcavity's optical modes, positioning these systems as promising candidates for reconfigurable photonic devices, optical switches, and sensors.

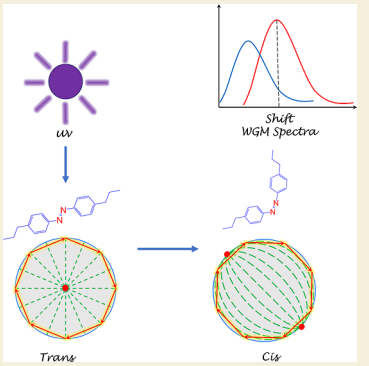

KEYWORDS: *whispering gallery mode, liquid crystals, azodendrimer, photoisomerism, all-optical switching*

INTRODUCTION

Solid dielectric microresonators, available in diverse geometries such as spheres,[1,2] cylinders,[3,4] disks,[5,6] and tori[7] have been extensively investigated due to their exceptional optical confinement and spectral selectivity.[8−13] These structures support a variety of photonic functionalities, including active optical filtering, all-optical switching, optical frequency comb generation, and cavity optomechanics.[14−22] Among the simplest and most widely studied are spherical microresonators, which confine light by total internal reflection at the dielectric boundary. In such systems, light circulates near the periphery of the resonator, and constructive interference occurs when the length of the round-trip optical path satisfies the relation $2\pi an \approx l\lambda$, where a is the radius of the microsphere, n is the refractive index of the sphere, l is the number of the polar modes, and λ is the wavelength. This condition defines the whispering gallery mode (WGM) resonance.[8] WGMs are characterized by low mode volumes and ultrahigh quality factors (Q), allowing prolonged photon lifetimes and enhanced light−matter interactions.[23]

A crucial feature for advancing integrated photonic technologies is tunability—the ability to dynamically respond in real time.[24−27] Despite their high Q factors, solid dielectric microresonators suffer from limited tunability because mode shifts require physical deformation or changes in the refractive index at the cavity interface, both of which pose practical challenges and tend to provide only small, often irreversible, spectral shifts. Liquid crystals (LCs) have emerged as an exceptional platform for tunable optical microcavities.[28−43] LCs exhibit stimuli-responsive molecular reorientation and morphology change under applied electric[43,44] and magnetic fields,[28] pressure,[11] or light.[45−48] Such external influences dynamically modulate the effective refractive index within LC droplets, enabling significant and reversible shifts in WGM resonance wavelengths. For example, a substantial tuning of WGMs in LC microcavity (~20 nm) by electric field and temperature have been reported by Humar et al.[49] and Sofi et al.[50] In ferromagnetic nematic microdroplets a magnetic field tuning of WGM modes (~1 nm/100 mT) have been demonstrated by Mur et al.[28] A highly sensitive pressure sensor (~20 mPa) based on the morphology dependent shift of the optical modes has been demonstrated by Manzo et al.[51−53] The intrinsic sensitivity of LCs to environmental changes makes them ideal candidates for tunable photonic devices and sensors.[54−57] Prior WGM tuning in LC droplets relied mainly on electric fields, temperature, magnetic fields, or pressure. In this work, we demonstrate all-optical reconfigurable WGM microcavities by introducing a novel, light-driven approach to dynamically tune WGM resonances in liquid crystal (LC) microdroplets doped with azodendrimer molecules. The azodendrimer photoisomerization[45−47] induces

Received: September 5, 2025
Revised: November 28, 2025
Accepted: December 5, 2025
Published: December 10, 2025

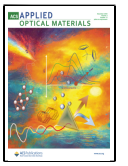

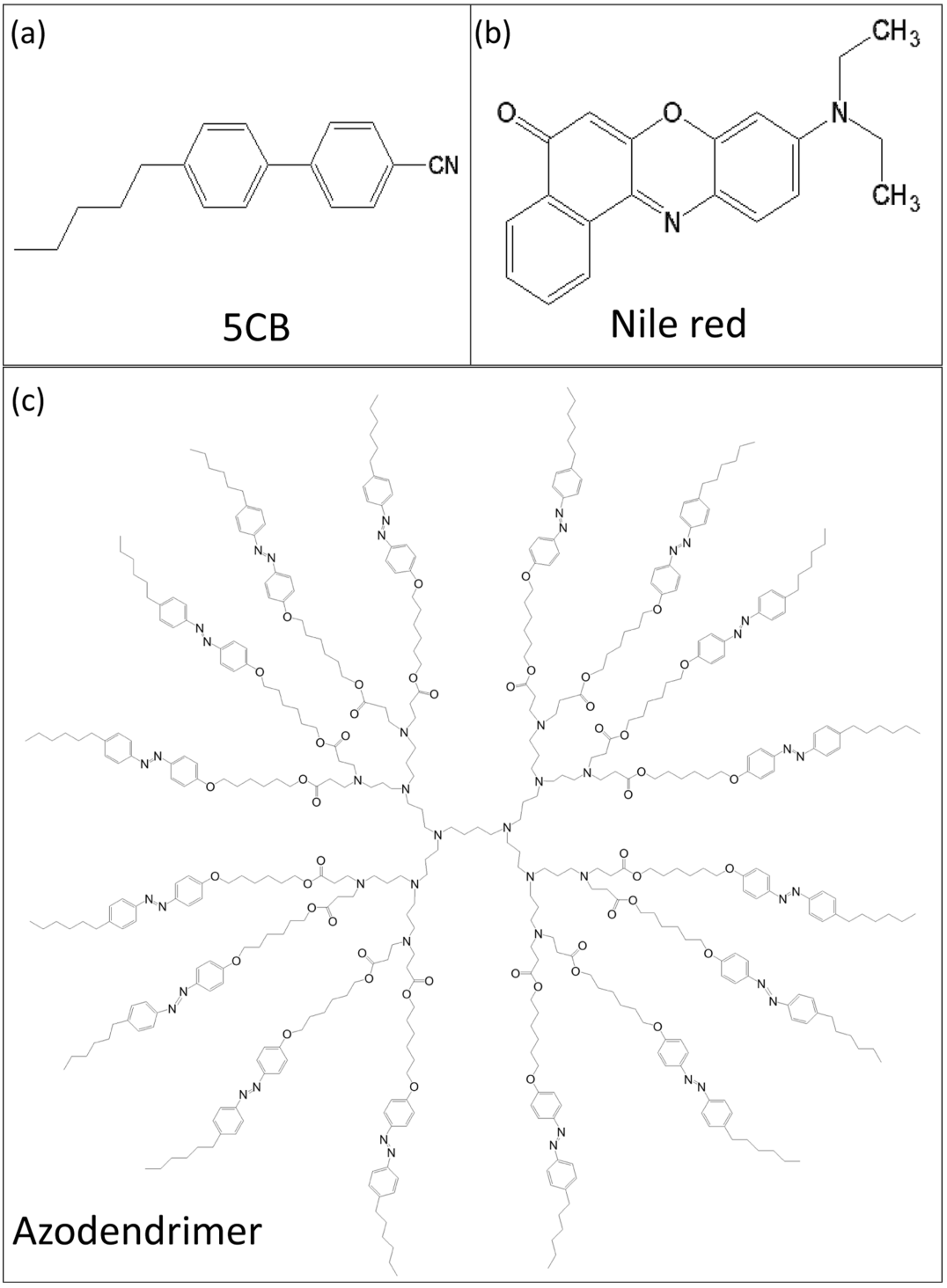

Figure 1. Molecular structures of (a) 5CB liquid crystal (b) Nile red and (c) Azodendrimer.

realignment of the LC director field and modifies droplet morphology in real time, resulting in rapid, reversible and noncontact control over the resonant modes.

RESULTS AND DISCUSSION

The 5CB nematic liquid crystal doped with azodendrimer and Nile red was mixed with lecithin doped glycerol (see Figure 1) and stirred gently to produce dispersed microdroplets. It forms microdroplets of varying size as shown in Figure 2c. The sample was exposed to ultraviolet (UV) light of wavelength 365 nm and intensity 4.5 mW/cm^2 to induce photoisomerization of the dopant molecules. Figure 2d shows that in the absence of UV illumination, suspended LC droplets exhibit a radial configuration in which the director is perpendicular to the LC−glycerol interface, containing a radial hedgehog defect in the center. Upon UV irradiation, the azodendrimer molecules undergo trans to cis isomerization, altering the interfacial anchoring from perpendicular to planar.[45,47,48] This drives a reorientation of the director from the radial state (Figure 2a) to a bipolar configuration, where

https://doi.org/10.1021/acsaom.5c00408
ACS Appl. Opt. Mater. 2025, 3, 2841−2847

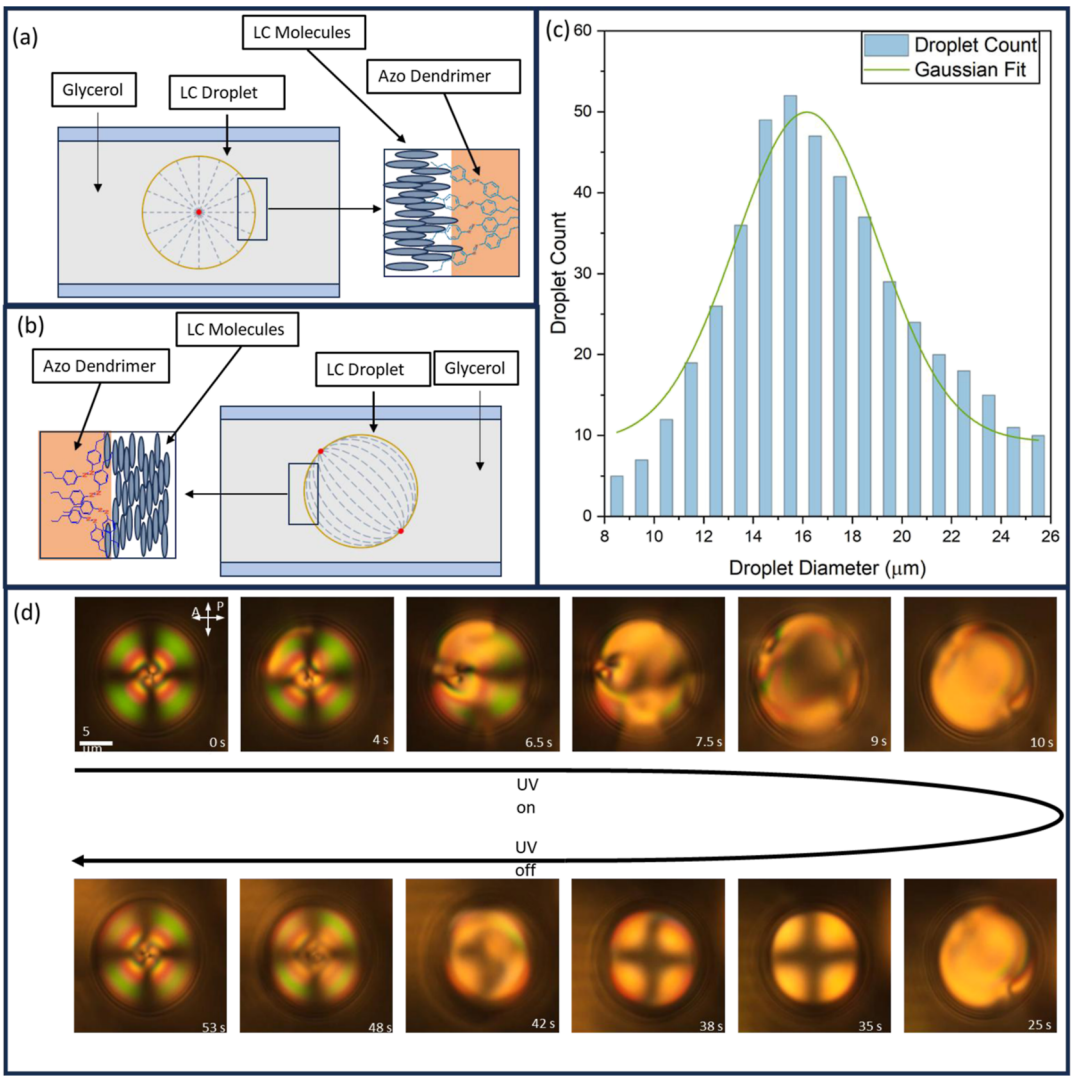

Figure 2. Schematic diagram of LC microdroplets showing (a) radial and (b) bipolar structure. The droplet with radial configuration induces a hedgehog at the center indicated by a red dot. The droplets with bipolar configuration induces antipodal surface boojums. The adjacent boxes highlight the interface of the LC and azodendrimer molecules. (c) Distribution of droplets size. (d) Polarizing optical microscope images of a 15 μm droplet under UV (365 nm) exposure. Top row shows the transition of the droplet from radial to bipolar when the UV light is turned on and the bottom row shows the reverse transition when the UV light is turned off.

the director lies tangentially parallel to the interface (Figure 2b). Transformation proceeds through transient states such as escaped radial and preradial textures as shown in Figure 2d. When UV light is turned off, the azodendrimer molecules revert to the trans form, restoring homeotropic anchoring and the radial droplet configuration. The defect topology also evolves accordingly. In particular, during the radial to bipolar transition, the central point defect migrates toward the periphery, where it splits open to form a pair of antipodal surface boojum defects. On returning to the radial state under visible light, the boojum defect collapses back into a single central point defect stabilizing radial configuration of the director. Thus, the structure of the microdroplet can be switched between these two configurations by repeatedly turning on and off UV light.

For optical characterization of WGM resonance, the pulsed laser was tightly focused onto the droplets. A typical image of an excited droplet of diameter 25 μm and its spectra is shown in Figure 3a. It supports several TE (Transverse Electric) and TM (Transverse Magnetic) modes with low free spectral range (FSR), making resonance tracking under UV illumination difficult. In smaller droplets, only TM modes experience a high enough refractive index contrast (extraordinary refractive index vs the external medium) to meet the resonance condition for strong total internal reflection, resulting in clear WGMs. As the droplet size increases, the light path inside the sphere becomes longer, meaning that even the lower refractive index contrast of the ordinary refractive index (which TE modes experience) becomes sufficient for resonance. Hence, in this work we used droplets with diameters much smaller than 25 μm for the analysis, which only supports the TM mode.

A droplet with a diameter of 15 μm was chosen for the WGM experiments. To prevent photobleaching of Nile Red molecules, each measurement used a short duration of (5 to 10 s) laser excitation. Emission spectra were recorded as the pump power was varied, and both the intensity and the full width at half-maximum (fwhm) of the brightest mode (l = 129) were analyzed as functions of the input power (Figure 3b). In particular, both intensity and peak width showed a distinct slope change at 0.6 μJ, revealing the lasing threshold for the

https://doi.org/10.1021/acsaom.5c00408
ACS Appl. Opt. Mater. 2025, 3, 2841−2847

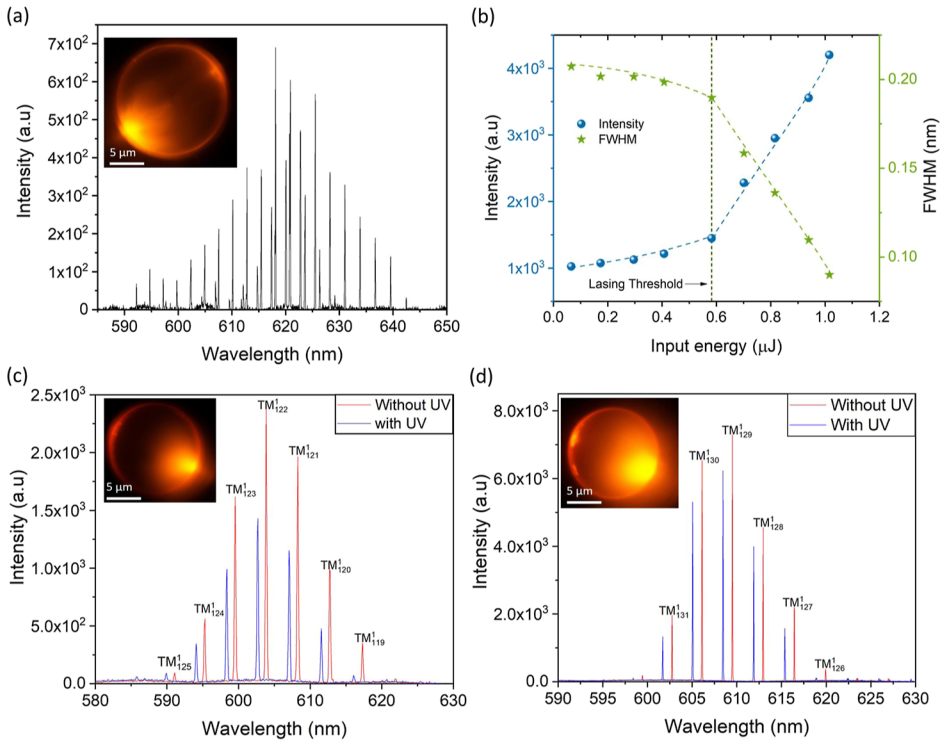

Figure 3. (a) WGM spectra of a microdroplet of diameter 25 μm. (b) Variation of the intensity and fwhm of the most intense mode (l = 129) as a function of pump energy of a droplet of diameter 15 μm. Vertical dotted line indicates threshold pump energy for lasing (~0.6 μJ). (c) WGM spectra of a droplet of diameter 14 μm with and without UV irradiation below the lasing threshold (pump energy 0.26 μJ). (d) WGM spectra of a droplet of diameter 15 μm above the lasing threshold pump energy (0.7 μJ). Insets show optical micrographs of the emission pattern on the droplets.

droplet. Below this threshold, the droplet supported only passive WGM resonances; above it, lasing commenced, indicating the onset of active emission behavior.

In what follows, we discuss the effect of UV exposure on the WGM resonances. The WGM spectra of two nematic LC droplets, having almost similar diameters (14 and 15 μm) are presented in Figure 3c,d. The 14 μm droplet (Figure 3c) was excited with an input energy of 0.26 μJ, which is well below its lasing threshold. The 15 μm droplet (Figure 3d) was excited with an energy of 0.7 μJ, which is just above the lasing threshold energy. Below the lasing threshold only a bright light ring in the periphery is observed. Above the threshold, additional red speckle, characteristic of coherent emission, is observed.[42,58] In both cases, only TM-polarized modes were detected. For TM polarization, the electric field is oriented perpendicular to the droplet interface, and the circulating light experiences the extraordinary refractive index (n_e) of the nematic LC. The polar mode numbers of the observed resonances were evaluated using the following resonant wavelength approximation for spherical microcavities with small radial mode numbers[59,60]

$$n_s ka = l - \alpha_q \left(\frac{l}{2}\right)^{1/3} - \frac{\chi n_r}{\sqrt{n_r^2 - 1}} + \frac{3\alpha_q^2}{20}\left(\frac{l}{2}\right)^{-1/3} - \frac{\alpha_q n_r \chi(2\chi^2 - 3n_r^2)}{6(n_r^2 - 1)^{3/2}}\left(\frac{l}{2}\right)^{-2/3} + O(l^{-1}) \quad (1)$$

where k is the wavenumber, a is the radius, $l \gg 1$, is the polar mode number, q = 1, 2, 3···is the radial mode number and $\chi = \frac{1}{n_r^2}$ for the TM modes while χ = 1 for the TE modes. α_q are the negative q-th zeros of the Airy function and $n_r = \frac{n_s}{n_a}$ is the refractive index ratio, where n_s is the refractive index of the surrounding medium and n_a is the refractive index of the microdroplets. From this analysis, the 14 μm droplet supports polar mode numbers ranging from l = 119 to 125 (Figure 3c), while the 15 μm droplet supports modes from l = 126 to 131 (Figure 3d). In the 14 μm droplet, the mode corresponding to l = 122 appears at 604 nm (without UV illumination) and shifts to 602 nm under UV illumination. That means that the mode shows a blue shift of 2 nm. In fact, all other modes are blue-shifted by a similar value. Similarly, for lasing in a 15 μm droplet, the mode l = 129 shifts from 609.5 nm (without UV illumination) to 608.4 nm (under UV illumination). Considering that the polar mode number l remains unchanged, under UV illumination, we estimate approximate change in the effective refractive index of the cavity from this mode shift using the first order approximation of eq 1, namely $n_{\text{eff}} = l\lambda_{\text{shifted}}/2\pi a$. For example, taking l = 122, shifted wavelength λ_{shifted} = 602.7 nm, the estimated effective refractive index n_{eff} = 1.66 is lower by 0.11 than the extraordinary refractive index n_e = 1.77 of 5CB at room temperature.[61] In addition, a pronounced reduction in the Q factor, obtained by fitting a Lorentzian function to the intensity profile, is also observed for passive WGM resonances during the UV-induced droplet reconfiguration. For example, without UV illumination, the Q factor of the 14 μm droplet lies in the range 3.5 × 10^3–4 × 10^3, and decreases to 2.5 × 10^3–3 × 10^3 under UV exposure. This reduction reflects increased scattering and mode broadening caused by director field and surface anchoring changes during the radial-bipolar transformation. In contrast, the Q

https://doi.org/10.1021/acsaom.5c00408
ACS Appl. Opt. Mater. 2025, 3, 2841−2847

factor of the lasing modes is significantly higher (~15×10^3) and shows a similar change under UV illumination.

Finally, we studied the reversibility of mode shift by subjecting a particular microdroplet to multiple cycles of laser excitation and UV irradiation. Figure 4 shows that the

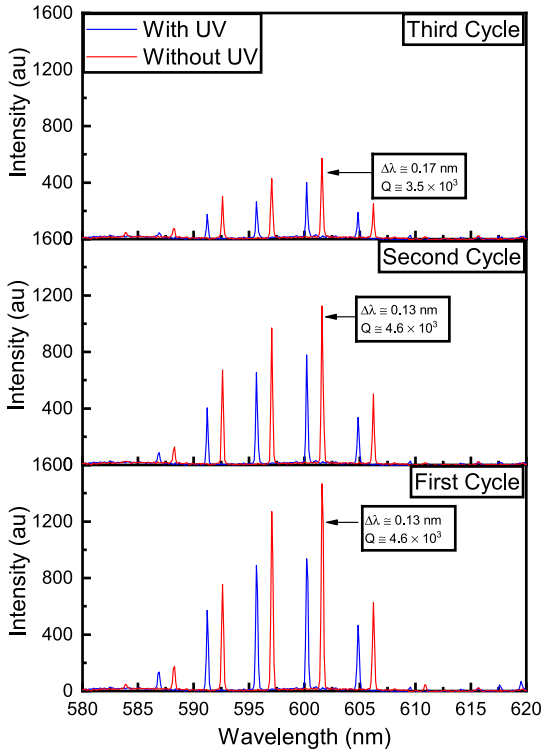

Figure 4. Effect of multiple cycles of laser excitation and UV irradiation on the WGM of a 15.5 μm droplet.

mode shift is almost unchanged (1.5 nm) throughout, and up to the second cycle the fwhm ($\Delta\lambda$) and the Q factor does not change appreciably, but in the third cycle there is a considerable change. For example, for the most intense mode (marked by an arrow), in the first and second cycles $\Delta\lambda \simeq 0.13$ nm and the corresponding quality factor $Q \simeq 4.5 \times 10^3$. In the third cycle, the peak intensity of the modes had decreased and the fwhm increased ($\Delta\lambda \simeq 0.17$ nm), consequently the quality factor decreased ($Q \simeq 3.5 \times 10^3$). Physically, the droplet looks the same as was formed and it transformed back and forth between radial to boojum structures under several UV exposures. Hence, the decrease in the intensity of the mode and the quality factor is not associated with any physical change in the cavity. It may be related to photobleaching of dye molecules and other losses in the cavity, which could be improved by choosing appropriate fluorescent dyes and liquid crystals. Here, two remarks are in order regarding our experiments. First, the droplets are prepared manually. Hence, it was difficult to produce droplets with exactly the same diameter across the samples. It mainly depends on the stirring conditions while the LC is dispersed in the polymer matrix. We attempted to maintain a uniform stirring condition, which resulted in droplets of varying sizes as shown in Figure 2c. Second, further studies are necessary to optimize the system to improve the reversibility of the resonance under repeated laser excitations and UV exposures for device applications.

CONCLUSION

We have demonstrated that doping nematic liquid crystal microdroplets with photoresponsive azodendrimer molecules enables an all-optical route for reversible optical tuning of whispering gallery modes. The trans−cis photoisomerization of the azodendrimer under controlled illumination reorients the liquid crystal director at the droplet interface, thereby altering the effective refractive index experienced by circulating light. This dynamic modulation of the refractive index results in measurable blue shifts of ~2 nm in the WGM spectra. Our findings show that light alone can be used as a noncontact, low-power control stimulus to modulate optical microcavities with high precision, without compromising structural integrity. We demonstrated molecular photoisomerization at the interface to cavity-index modulation in situ, establishing a generalizable route for photonic tuning via surface anchoring chemistry. The approach combines the high-Q confinement of

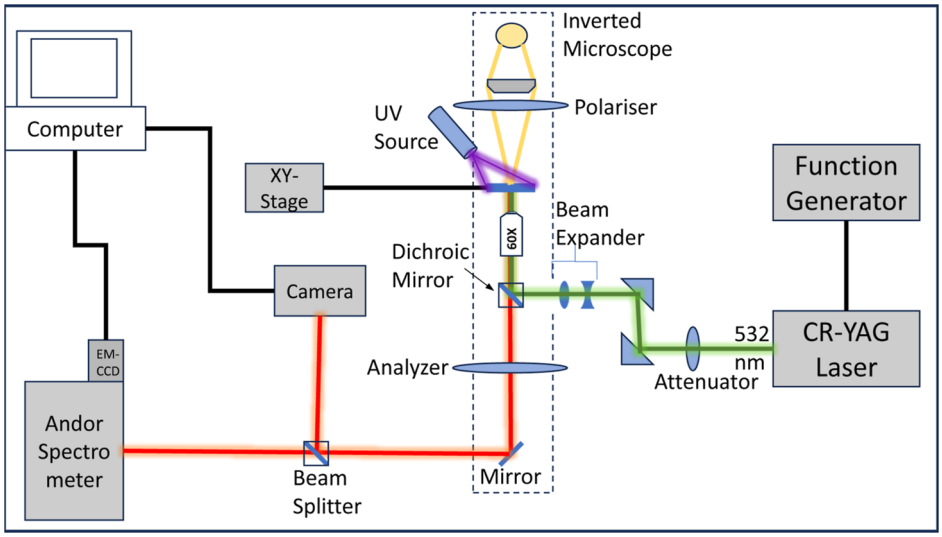

Figure 5. Experimental setup to study WGM resonance of LC microdroplets. It is build around an inverted microscope. The droplets were exposed to the UV light from the top.

https://doi.org/10.1021/acsaom.5c00408
ACS Appl. Opt. Mater. 2025, 3, 2841−2847

spherical LC microresonators with molecular-level photoresponsivity, offering a versatile route toward reconfigurable microlasers, optical switches, and high-performance sensors. Beyond demonstrating a proof-of-principle platform, this work opens opportunities for integrating photoresponsive soft matter into tunable photonic architectures, enabling compact, adaptive devices driven entirely by optical stimuli.

EXPERIMENTAL SECTION

The nematic liquid crystal 4-cyano-4′-pentylbiphenyl (5CB) (extraordinary refractive index n_e = 1.77, ordinary refractive index n_e = 1.58 at 25 °C) was used as host medium (Figure 1a). LC was doped with 0.1 wt % azodendrimer, a photochromic molecule containing multiple azobenzene units (Figure 1c). In the absence of UV illumination, the azodendrimer molecules predominantly adopt the trans configuration; exposure to ultraviolet light induces reversible *trans*-to *cis*-isomerization. UV irradiation was provided by a CoolLED PE 300 (Nikon) source. To facilitate laser excitation and probing of whispering gallery modes, the LC mixture was further doped with 0.1 wt % Nile Red (Figure 1b) having absorption maximum at 550 nm and emission in the visible spectral range.[62] The liquid crystal microdroplets were prepared by dispersing the LC microdroplets into glycerol (refractive index 1.47) within a rectangular glass chamber (1 cm × 1 cm × 200 μm), prepared by double-sided adhesive tape attached to a clean glass microscope slide. The chamber was subsequently sealed with a coverslip to prevent evaporation and contamination. This procedure yields stable, isolated nematic LC microdroplets suspended in glycerol that are suitable for optical characterization.

The experimental arrangement to study WGM resonances was built around an inverted optical microscope (Nikon Ti2) as shown in Figure 5. A 60× water-immersion objective (NA = 1.0) was used both for imaging and to focus the excitation beam onto the liquid crystal microdroplets. The droplet textures were observed in real time using a color camera (Nikon DS-Ri2) mounted on the microscope. Laser excitation was provided by a pulsed Nd/YAG microchip laser with a repetition rate of 20 Hz (Teem Photonics PNG-02010, pulse width = 400 ps, wavelength = 532 nm). The beam was tightly focused onto the microdroplet through the objective. The experiments were carried out in a pump pulse energy range of 0.1 to 1 μJ. Fluorescence emission from the droplets, including WGM signals, was collected through the same objective and separated from the pump beam using a dichroic mirror positioned beneath the objective turret. The diverted light was directed to a Czerny−Turner spectrometer (Andor Shamrock 500i, focal length = 500 mm) equipped with a 1200 lines/mm diffraction grating blazed near 500 nm, matching the emission spectrum of Nile Red. This grating provided a spectral resolution of 0.07 nm. All measurements were performed at a controlled temperature of 25 °C to maintain stable liquid crystal phase and optical properties.

AUTHOR INFORMATION

Corresponding Author

Surajit Dhara − *School of Physics, University of Hyderabad, Hyderabad 500046, India;* orcid.org/0000-0003-3144-0300; Email: surajit@uohyd.ac.in

Authors

Asish P. Venkitesh − *School of Physics, University of Hyderabad, Hyderabad 500046, India;* orcid.org/0009-0002-3521-4861

Ramesh Manda − *School of Physics, University of Hyderabad, Hyderabad 500046, India*

Osamu Haba − *Graduate School of Organic Materials Science, Yamagata University, Yonezawa 992-8510, Japan*

Complete contact information is available at: https://pubs.acs.org/10.1021/acsaom.5c00408

Notes

The authors declare no competing financial interest.

ACKNOWLEDGMENTS

APV and SD acknowledge financial support from the Institute of Eminence, University of Hyderabad (UoH/IoE/RC1-20-010). RM acknowledges Ramanujan Fellowship (RJF/2022/000094) of Anusandhan National Research Foundation.

REFERENCES

(1) Gorodetsky, M. L.; Grudinin, I. S. Fundamental thermal fluctuations in microspheres. *J. Opt. Soc. Am. B* **2004**, *21*, 697−705.

(2) Matsko, A. B.; Savchenkov, A. A.; Yu, N.; Maleki, L. Whispering-gallery-mode resonators as frequency references. I. Fundamental limitations. *J. Opt. Soc. Am. B* **2007**, *24*, 1324−1335.

(3) Balistreri, M. L. M.; Klunder, D. J. W.; Blom, F. C.; Driessen, A.; Hoekstra, H. W. J. M.; Korterik, J. P.; Kuipers, L.; van Hulst, N. F. Visualizing the whispering gallery modes in a cylindrical optical microcavity. *Opt. Lett.* **1999**, *24*, 1829−1831.

(4) Mei, Y.; Wang, D. N.; Wang, Q.; Zhang, Y. Optical fiber integrated WGM cylindrical cavity resonator. *Opt. Lett.* **2024**, *49*, 4609−4612.

(5) Ryu, H.; Notomi, M.; Kim, G.; Lee, Y. High quality-factor whispering-gallery mode in the photonic crystal hexagonal disk cavity. *Opt. Exp.* **2004**, *12*, 1708−1719.

(6) Balac, S.; Dauge, M.; Dumeige, Y.; Féron, P.; Moitier, Z. Mathematical analysis of whispering gallery modes in graded index optical micro-disk resonators. *Eur. Phys. J. D* **2020**, *74*, 221.

(7) Ohana, T. S.; Guendelman, G.; Mishuk, E.; Kandel, N.; Garti, D.; Gurovich, D.; Bitton, O.; Dayan, B. Design and fabrication of ultrahigh Q chip-based silica WGM micro-resonators for single-atom cavity-QED. *Opt. Exp.* **2024**, *32*, 43974−43986.

(8) Vahala, K. J. *Optical Microcavities*; World Scientific, 2004.

(9) Arnold, S.; Holler, S.; Druger, S. D. Optical Processes in Microcavities. In *Advanced Series in Applied Physics*; Chang, R. K., Campillo, A. J., Eds.; World Scientific, 1996; Vol. *Vol.3*.

(10) Vahala, K. Optical microcavities. *Nature* **2003**, *424*, 839−846.

(11) Jiang, X.; Qavi, A. J.; Huang, S. H.; Yang, L. Whispering-gallery sensors. *Matter* **2020**, *3*, 371−392.

(12) Matsko, A. B.; Ilchenko, V. S. Optical resonators with whispering-gallery modes-part I: basics. *IEEE J. Sel. Top. Quantum Electron.* **2006**, *12*, 3−14.

(13) Ilchenko, V. S.; Matsko, A. B. Optical resonators with whispering-gallery modes-part II: applications. *IEEE J. Sel. Top. Quantum Electron.* **2006**, *12*, 15−32.

(14) Vollmer, F.; Arnold, S. Whispering-gallery-mode biosensing: label-free detection down to single molecules. *Nat. Methods* **2008**, *5*, 591−596.

(15) Yang, J. J.; Huang, M.; Dai, X. Z.; Huang, M. Y.; Liang, Y. A. A spoof surface WGM sensor based on a textured PEC cylinder. *Euro. Phys. Lett.* **2013**, *103*, 44001.

(16) Arnold, S.; ShopovaHoller, S. I.; Holler, S. Whispering gallery mode bio-sensor for label-free detection of single molecules: thermo-optic vs. reactive mechanism. *Opt. Exp.* **2009**, *18*, 281.

(17) Arnold, S.; Khoshsima, M.; Teraoka, I.; Holler, S.; Vollmer, F. Shift of whispering-gallery modes in microspheres by protein adsorption. *Opt. Lett.* **2003**, *28*, 272−274.

(18) Vollmer, F.; Arnold, S.; Keng, D. Single virus detection from the reactive shift of a whispering-gallery mode. *Proc. Natl. Acad. Sci. (USA)* **2008**, *105*, 20701−20704.

(19) Fan, X.; White, I. M.; Shopova, S. I.; Zhu, H.; Suter, J. D.; Sun, Y. Sensitive optical biosensors for unlabeled targets: a review. *Anal. Chim. Acta* **2008**, *620*, 8−26.

(20) Loncar, M. Molecular sensors: Cavities lead the way. *Nat. Photonics* **2007**, *1*, 565−567.

(21) Wang, H.; Yuan, L.; Kim, C. W.; Han, Q.; Wei, T.; Lan, X.; Xiao, H. Optical microresonator based on hollow sphere with porous wall for chemical sensing. *Opt. Lett.* **2012**, *37*, 94−96.

(22) He, L.; Ozdemir, S. K.; Zhu, J.; Kim, W.; Yang, L. Detecting single viruses and nanoparticles using whispering gallery microlasers. *Nat. Nanotechnol.* **2011**, *6*, 428−432.
(23) Banad, Y. M.; Hasan, S. M. A.; Sharif, S. S.; Veronis, G.; Gartia, M. R. Optical properties and behavior of whispering gallery mode resonators in complex microsphere configurations: Insights for sensing and information processing applications. *Nano Select* **2024**, *5*, 2300184.
(24) Lin, S.; Gutierrez-Cuevas, K. G.; Zhang, X.; Guo, J.; Li, Q. Fluorescent Photochromic α-Cyanodiarylethene Molecular Switches: An Emerging and Promising Class of Functional Diarylethene. *Adv. Funct. Mater.* **2021**, *31*, 2007957.
(25) Hu, H.; Liu, B.; Li, M.; Zheng, Z.; Zhu, W. A Quadri-Dimensional Manipulable Laser with an Intrinsic Chiral Photoswitch. *Adv. Mater.* **2022**, *34*, 2110170.
(26) Shi, Y.; Han, J.; Jin, X.; Miao, W.; Zhang, Y.; Duan, P. Chiral Luminescent Liquid Crystal with Multi-State-Reversibility: Breakthrough in Advanced Anti-Counterfeiting Materials. *Adv. Sci.* **2022**, *9*, 2201565.
(27) Hou, J.; Toyoda, R.; Meskers, S. C. J.; Feringa, B. L. Programming and Dynamic Control of the Circular Polarization of Luminescence from an Achiral Fluorescent Dye in a Liquid Crystal Host by Molecular Motors. *Angew. Chem., Int. Ed.* **2022**, *61*, No. e202206310.
(28) Mur, M.; Sofi, J. A.; Kvasić, I.; Mertelj, A.; Lisjak, D.; Niranjan, V.; Muševič, I.; Dhara, S. Magnetic-field tuning of whispering gallery mode lasing from ferromagnetic nematic liquid crystal microdroplets. *Opt. Exp.* **2017**, *25*, 1073−1083.
(29) Ioppolo, T.; Kozhevnikov, M.; Stepaniuk, V.; Ötügen, M. V.; Sheverev, V. Micro-optical force sensor concept based on whispering gallery mode resonators. *Appl. Opt.* **2008**, *47*, 3009−3014.
(30) Wang, D.; Rong, J.; Li, J.; Yue, H.; Liu, W.; Xing, E.; Tang, J.; Liu, J. Highly sensitive force sensor based on high-Q asymmetric V-shaped CaF_2 resonator. *Micromachines* **2024**, *15*, 751.
(31) Humar, M.; Muševič, I. Surfactant sensing based on whispering-gallery-mode lasing in liquid-crystal microdroplets. *Opt. Exp.* **2011**, *19*, 19836.
(32) Jampani, V. S.; Humar, M.; Muševič, I. Resonant transport of light from planar polymer waveguide into liquid-crystal microcavity. *Opt. Exp.* **2013**, *21*, 20506−20516.
(33) Sofi, J. A.; Dhara, S. Stability of liquid crystal based optical microresonators. *Liq. Cryst.* **2019**, *46*, 629−639.
(34) Muševič, I.; Skarabot, M.; Humar, M. Direct and inverted nematic dispersions for soft matter photonics. *J. Phys.: Condens. Matter* **2011**, *23*, 284112.
(35) Giorgini, A.; Avino, S.; Malara, P.; De Natale, P.; Gagliardi, G. Fundamental limits in high-Q droplet microresonators. *Sci. Rep.* **2017**, *7*, 41997.
(36) Lee, C. R.; Lin, J. D.; Huang, B. Y.; Mo, T. S.; Huang, S. Y. All-optically controllable random laser based on a dye-doped liquid crystal added with a photoisomerizable dye. *Opt. Exp.* **2010**, *18*, 25896−25905.
(37) Shibaev, P. V.; Crooker, B.; Manevich, M.; Hanelt, E. Mechanically tunable microlasers based on highly viscous chiral liquid crystals. *Appl. Phys. Lett.* **2011**, *99*, 233302.
(38) Lin, J. D.; Hsieh, M. H.; Wei, G. J.; Mo, T. S.; Huang, S. Y.; Lee, C. R. Optically tunable/switchable omnidirectionally spherical microlaser based on a dye-doped cholesteric liquid crystal micro-droplet with an azo-chiral dopant. *Opt. Exp.* **2013**, *21*, 15765−15776.
(39) Humar, M.; Muševič, I. 3D microlasers from self-assembled cholesteric liquid-crystal microdroplets. *Opt. Exp.* **2010**, *18*, 26995−27003.
(40) Kumar, T. A.; Mohiddon, M. A.; Dutta, N.; Viswanathan, N. K.; Dhara, S. Detection of phase transitions from the study of whispering gallery mode resonance in liquid crystal droplets. *Appl. Phys. Lett.* **2015**, *106*, 051101.
(41) Sofi, J. A.; Dhara, S. Electrically switchable whispering gallery mode lasing from ferroelectric liquid crystal microdroplets. *Appl. Phys. Lett.* **2019**, *114*, 091106.
(42) Sofi, J. A.; Barthakur, A.; Dhara, S. Whispering gallery mode lasing in mesomorphic liquid crystal microdroplets. *Soft Matter* **2019**, *15*, 7832−7837.
(43) Venkitesh, A. P.; Barthakur, A.; Kula, P.; Dhara, S. Two-way tuning of whispering gallery mode resonance of dual-frequency nematic liquid crystal microdroplets. *ACS Appl. Opt. Mater.* **2024**, *2* (12), 2605−2611.
(44) Humar, M. Liquid-crystal-droplet optical microcavities. *Liq. Cryst.* **2016**, *43*, 1937−1950.
(45) Lee, G.; Araoka, F.; Ishikawa, K.; Momoi, Y.; Haba, O.; Yonetake, K.; Takezoe, H. Photoinduced ordering transition in microdroplets of liquid crystals with azo-dendrimer. *Part. Part. Syst. Charact.* **2013**, *30*, 847−852.
(46) Shvetsov, S. A.; Emelyanenko, A. V.; Boiko, N. I.; Liu, J.-H.; Khokhlov, A. R. Communication: Orientational structure manipulation in nematic liquid crystal droplets induced by light excitation of azodendrimer dopant. *J. Chem. Phys.* **2017**, *146*, 211104.
(47) Eremin, A.; Nádasi, H.; Hirankittiwong, P.; Kiang-Ia, J.; Chattham, N.; Haba, O.; Yonetake, K.; Takezoe, H. Azodendrimers as a photoactive interface for liquid crystals. *Liq. Cryst.* **2018**, *45*, 2121−2131.
(48) Noh, J.; Jampani, V. S. R.; Haba, O.; Yonetake, K.; Takezoe, H.; Lagerwall, J. P. F. Sub-second dynamic phototuning of alignment in azodendrimer-doped nematic liquid crystal shells. *J. Mol. Liq.* **2018**, *267*, 197−204.
(49) Humar, M.; Ravnik, M.; Pajk, S.; Muševič, I. Electrically tunable liquid crystal optical microresonators. *Nat. Photonics* **2009**, *3*, 595−600.
(50) Sofi, J. A.; Mohiddon, M. A.; Dutta, N.; Dhara, S. Electrical and thermal tuning of quality factor and free spectral range of optical resonance of nematic liquid crystal microdroplets. *Phys. Rev. E* **2017**, *96*, 022702.
(51) Manzo, M.; Ioppolo, T.; Ayaz, U. K.; LaPenna, V.; Ötügen, M. V. A photonic wall pressure sensor for fluid mechanics applications. *Rev. Sci. Instrum.* **2012**, *83* (10), 105003.
(52) Madugani, R.; Yang, Y.; Le, V. H.; Ward, J. M.; Nic Chormaic, S. Linear Laser Tuning Using a Pressure-Sensitive Microbubble Resonator. *IEEE Photon. Technol. Lett.* **2016**, *28* (10), 1134−1137.
(53) Yang, Y.; Saurabh, S.; Ward, J. M.; Nic Chormaic, S. High-Q, ultrathin-walled microbubble resonator for aerostatic pressure sensing. *Opt. Exp.* **2016**, *24*, 294.
(54) Yang, X.; Tang, S.; Meng, J.; Zhang, P.; Chen, Y.; Xiao, Y. Phase-Transition Microcavity laser. *Nano Lett.* **2023**, *23* (7), 3048−3053.
(55) Wang, J.; Song, Y.; Dou, X.; Sun, J.; Yang, X.; Zhang, Y.; Liu, Z.; Li, Y.; Li, H. Liquid crystal microcavity biosensors for real-time liver injury monitoring via whispering gallery mode laser. *Research* **2025**, *8*, 0824.
(56) Duan, R.; Hao, X.; Li, Y.; Li, H. Detection of acetylcholinesterase and its inhibitors by liquid crystal T biosensor based on whispering gallery mode. *Sens. Actuators, B* **2020**, *308*, 127672.
(57) Tsao, Y.; Chen, H.; Chen, Y. Electrically tunable coupling between band-edge lasing and whispering gallery modes in liquid crystal microdroplets. *Adv. Opt. Mater.* **2025**, *13*, 2403124.
(58) Draijer, M.; Hondebrink, E.; van Leeuwen, T.; Steenbergen, W. Review of laser speckle contrast techniques for visualizing tissue perfusion. *Lasers. Med. Sci.* **2009**, *24* (4), 639−651.
(59) Lam, C. C.; Leung, P. T.; Young, K. Explicit asymptotic formulas for the positions, widths, and strengths of resonances in Mie scattering. *J. Opt. Soc. Am. B* **1992**, *9*, 1585−1592.
(60) Schiller, S. Asymptotic expansion of morphological resonance frequencies in Mie scattering. *Appl. Opt.* **1993**, *32*, 2181−2185.
(61) Karat, P. P.; Madhusudana, N. V. Elasticoty and orientational order in some 4'-n-alkyl-4-cyanobiphenyls. *Mol. Cryst. Liq. Cryst.* **1976**, *36*, 51.
(62) Greenspan, P.; Fowler, S. D. Spectrofluorometric studies of the lipid probe, nile red. *J. Lipid Res.* **1985**, *26* (7), 781−789.

https://doi.org/10.1021/acsaom.5c00408
ACS Appl. Opt. Mater. 2025, 3, 2841−2847